

# Chemically-fueled phase transition of a redox-responsive polymer

Takafumi Enomoto<sup>a</sup>, Aya M. Akimoto<sup>b</sup> and Ryo Yoshida<sup>a</sup>

<sup>a</sup>Department of Materials Engineering, School of Engineering, The University of Tokyo, Bunkyo-ku, Japan;

<sup>b</sup>Department of Human-Centered Engineering, Faculty of Transdisciplinary Engineering, Ochanomizu University, Bunkyo-ku, Japan

## ABSTRACT

In living systems, dynamic biomacromolecular assemblies are driven and regulated by energy dissipative chemical reaction networks, enabling various autonomous functions. Inspired by this biological principle, we report a chemically-fueled phase transition of a poly(*N*-isopropylacrylamide) (PNIPAAm)-based polymer bearing viologen units (P(NIPAAm-V)), wherein redox changes drive coil-to-globule phase transitions. Upon the addition of a reducing agent, viologen moieties in P(NIPAAm-V) are converted into their reduced state, resulting in enhanced hydrophobicity and polymer aggregation. Coexistence of a platinum catalyst couples these redox-driven structural changes to hydrogen evolution, which oxidizes the viologen radicals, thus restoring the polymer chains to their hydrated random coil state. As a result, transient polymer assemblies form and subsequently disassemble upon depletion of the reducing agent, leading to a temporally controlled out-of-equilibrium phase transition. Moreover, by tuning the platinum concentration and reaction temperature, we achieve precise control of both the size and lifetime of these assemblies. Notably, viologen moieties constitute only about 1% of the polymer repeating units, underscoring that chemically-fueled phase transition is efficient strategy for dynamically regulating molecular assemblies. These findings demonstrate that chemically-fueled phase transitions in redox-responsive polymers offer a promising blueprint for designing dynamic, biomimetic materials capable of spatiotemporally regulated structural transformations.

## ARTICLE HISTORY

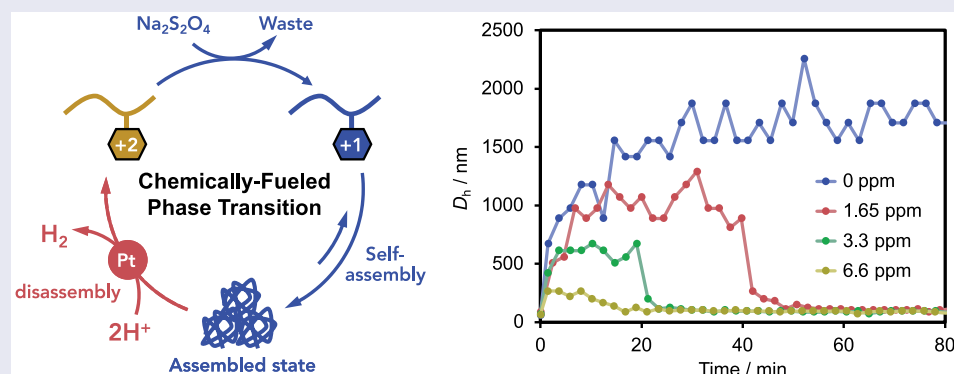
Received 30 January 2025

Accepted 12 April 2025

Revised 2 April 2025

## KEYWORDS

Chemically-fueled self-assembly; coil-to-globule phase transition; poly(*N*-isopropylacrylamide); hydrogen evolution; viologen





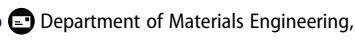
## IMPACT STATEMENT


By coupling a redox-responsive poly(*N*-isopropylacrylamide) derivative with platinum-catalyzed hydrogen evolution, this study establishes a chemically-fueled phase transition, paving the way for dynamic, energy-dissipative polymeric materials with tunable lifetimes and structural transformations reminiscent of biological systems.

## Introduction

In living systems, a wide variety of dynamic biomacromolecular assemblies display diverse functionalities that are finely regulated by complex chemical reaction networks [1–3]. For example, actin filaments, which are crucial for muscle tissues, undergo dynamic control of their length and spatial distribution through

ATP-mediated activation and deactivation processes, thereby playing an important role in cellular motion [4–6]. In this ATP-driven process, actin monomers bound to ATP easily self-assemble into actin filaments, and ATP is subsequently hydrolyzed to ADP by actin. This hydrolysis induces a conformational change in actin and enhances the dissociation of actin

**CONTACT** Takafumi Enomoto  [enomoto@cross.t.u-tokyo.ac.jp](mailto:enomoto@cross.t.u-tokyo.ac.jp); Ryo Yoshida  [ryo@cross.t.u-tokyo.ac.jp](mailto:ryo@cross.t.u-tokyo.ac.jp) 

 Supplemental data for this article can be accessed online at <https://doi.org/10.1080/14686996.2025.2494496>

© 2025 The Author(s). Published by National Institute for Materials Science in partnership with Taylor & Francis Group.

This is an Open Access article distributed under the terms of the Creative Commons Attribution-NonCommercial License (<http://creativecommons.org/licenses/by-nc/4.0/>), which permits unrestricted non-commercial use, distribution, and reproduction in any medium, provided the original work is properly cited. The terms on which this article has been published allow the posting of the Accepted Manuscript in a repository by the author(s) or with their consent.

monomers from the filament, leading to a kinetically regulated filament size. Such non-equilibrium self-assembly processes, which consume the chemical energy of high-energy molecules, are broadly referred to as chemically-fueled self-assembly. Chemically-fueled self-assembly plays critical roles in controlling the dynamics of various biomacromolecules in living systems [7–9]. By contrast, artificially designed polymeric systems that dynamically control their structures via chemical reaction cycles, similar to biomacromolecules, remain limited. To construct dynamic molecular assembly systems analogous to those in living organisms, an important strategy is to harness chemical reactions to actively regulate the assembly/disassembly states of molecular systems.

Recent studies have demonstrated that the incorporation of energy-dissipative chemical cycles can modulate self-assembly states [10–12]. A representative example utilizes carbodiimide-fueled self-assembly, where carbodiimide is hydrolyzed while converting carboxylic acids into their corresponding anhydrides in water [13–17]. These transient anhydrides are more hydrophobic than the precursor carboxylic acids and thus self-assemble. Because the anhydrides gradually hydrolyze back to carboxylic acids in water, these assemblies eventually disassemble, displaying a dissipative and transient nature reminiscent of ATP-driven processes in cells. Many chemically-fueled self-assembly systems composed of oligopeptides [13,14], aromatic compounds [15], and amphiphiles [16,17] have been realized using this approach, which is reminiscent of ATP-driven processes in biological systems. Beyond carbodiimide chemistry, various chemically-fueled self-assembly systems based on redox reactions [18–20], photoacid generation [21,22], and even ATP hydrolysis [23,24] have also been reported. Nevertheless, most of these systems rely on small-molecule building blocks (molecular weight up to 1000), leaving a substantial gap compared to the dynamic regulation of large biomacromolecules in living organisms. This discrepancy remains a major obstacle to designing artificial materials that manifest biomimetic, dynamic functions on macromolecular scales. Achieving efficient structural transitions with minimal driving force, as in natural proteins, is key to replicating the dynamic functions observed in biology.

A promising strategy to induce large structural changes with minor stimuli lies in the phase transitions of polymers in solution [25–27]. For instance, poly(*N*-isopropylacrylamide) (PNIPAAm) undergoes a well-known thermoresponsive coil-to-globule transition in water at around 32 °C [28–30]. Below 32 °C, PNIPAAm chains remain hydrated in a random coil state, whereas above 32 °C, they rapidly dehydrate, collapsing into globules. Furthermore, the introduction of various stimuli-responsive moieties into

PNIPAAm at a few percent content enables the design of diverse PNIPAAm-based polymers that respond to weak stimuli, closely emulating protein-like responsiveness [31–33]. Because this polymer allows reversible structural changes with minimal energy input, PNIPAAm-based stimuli-responsive systems can serve as synthetic models of marginally stable proteins, which readily change their conformations upon slight perturbations.

In this study, we combine the structural phase transition behavior of PNIPAAm-based polymers with chemical reaction cycles to establish chemically-fueled phase transition powered by reducing agents. Specifically, our approach employs a PNIPAAm derivative bearing viologen units (P(NIPAAm-V)) in conjunction with a platinum catalyst that mediates hydrogen evolution from water under acidic conditions (Figure 1). In our previous report, we demonstrated that incorporating a viologen moiety into PNIPAAm imparts a redox-responsive coil-to-globule phase transition, wherein the polymer's aggregation state changes according to the oxidation states of viologen [34,35]. Furthermore, viologen and its analogues are well-known electron mediators; when reduced viologen coexists with a platinum (Pt)-based catalyst under acidic conditions, electrons transfer from the reduced viologen to the platinum catalyst, producing hydrogen gas [36,37]. Hence, in the

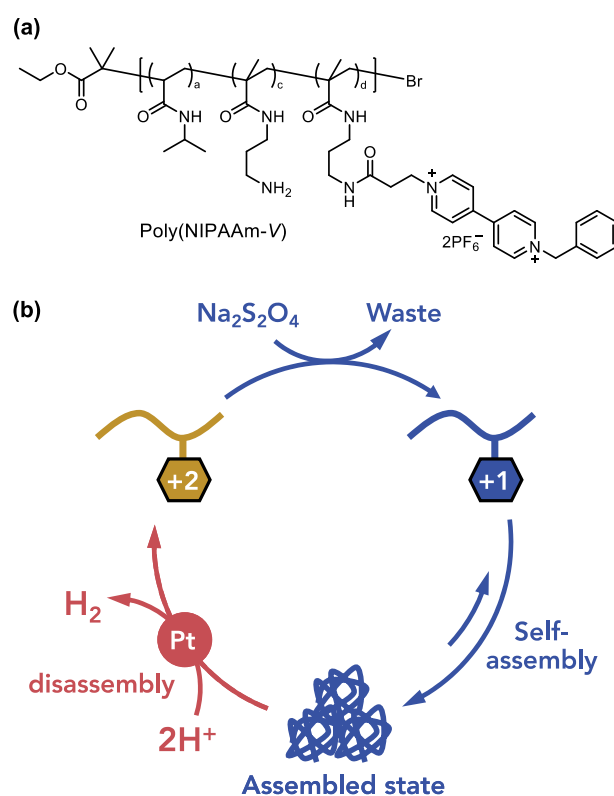


**Figure 1.** (a) Chemical structure of poly(NIPAAm-V). (b) Schematic illustration of chemically-fueled phase transition of a poly(NIPAAm-V) driven by a catalytic hydrogen evolution reaction.

presence of a reducing agent as the fuel, P(NIPAAm-V) undergoes a coil-to-globule transition upon reduction of viologen units. Subsequently, electron transfer from viologen to Pt catalyst drives hydrogen evolution, oxidizing viologen units back to their initial state. This reaction cycle drives the chemically-fueled phase transition, resulting in transient growth of polymer assemblies, the formation of a quasi-steady-state, and eventual re-dispersion of the assemblies once the fuel is depleted (Figure 1). Notably, by adjusting the concentration of the platinum catalyst, we are able to regulate the lifetime and size of these polymer assemblies. Because viologen units comprise only about 1% of the polymer chain, our system demonstrates that small redox changes can effectively induce large-scale transformations in high molecular weight polymers. Overall, the present findings underscore the potential of chemically-fueled phase transition strategies for constructing dynamic functional materials.

## Materials and methods

### Materials

*N*-isopropylacrylamide (NIPAAm) was kindly donated by KJ chemicals Co. (Tokyo, Japan) and purified by recrystallization from a toluene/hexane mixed solvent. *N*-(3-aminopropyl)methacrylamide (NAPMAm) was purchased from Combi-Blocks (San Diego, U.S.A.) and purified by reprecipitation from methanol into a large excess of tetrahydrofuran. All other chemical reagents

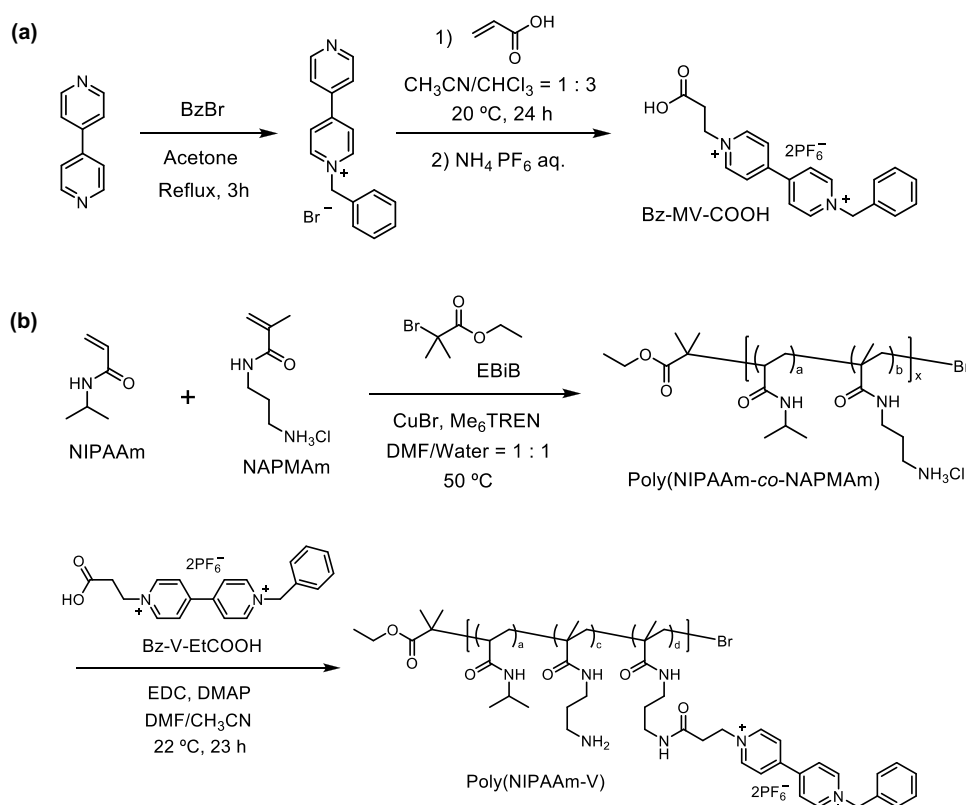
were purchased from FUJIFILM Wako Pure Chemical Co. (Osaka, Japan), Tokyo Chemical Industry Co. (Tokyo, Japan), or Sigma-Aldrich Co. LLC (Missouri, U.S.A.) and used as received.

### General methods

<sup>1</sup>H-NMR spectra were collected at room temperature using a JEOL JNM-ECS400 spectrometer (Tokyo, Japan). UV – Vis absorption spectra were measured on a SHIMADZU UV1900i spectrophotometer (Kyoto, Japan). DLS experiments were performed using an Otsuka Electronics ELSZ-2000 system (Osaka, Japan) equipped with a semiconductor laser (658 nm). The collected data were analyzed using the Contin fitting method. Evolved hydrogen gas was analyzed using a Shimadzu GC-2014 gas chromatograph (Kyoto, Japan) (molecular sieve 5A column; Ar carrier gas) equipped with a thermal conductivity detector, which was calibrated with standard hydrogen gas.

### Synthesis of *N*-(2-carboxyethyl)-*N'*-benzyl-4,4'-bipyridinium hexafluorophosphate (Bz-V-EtCOOH)

Bz-V-EtCOOH was synthesized according to the literatures [38,39] with modifications (Scheme 1(a)). A round-bottom flask was charged with 4,4'-bipyridine (16 g; 102 mmol) and dehydrated acetone (200 mL), and purged with Ar. Benzyl bromide (25



**Scheme 1.** (a) Synthesis of Bz-V-EtCOOH. (b) Synthesis of poly(NIPAAm-V).

mL; 102 mmol) was then added dropwise to the solution under Ar flow at room temperature. The reaction mixture was stirred for 3 h at 60 °C. After cooling the reaction mixture to room temperature, the precipitate was filtered and washed by acetone 3 times. The obtained solid was dried in vacuum to afford 1-benzyl-4,4'-bipyridinium bromide (33 g, 101 mmol, 99% yield). <sup>1</sup>H-NMR (DMSO-*d*<sub>6</sub>; 400 MHz):  $\delta$  = 9.38 (d, *J* = 6.9 Hz, 2H, Bz-py<sup>+</sup>), 8.87 (d, *J* = 6.0 Hz, 2H, py), 8.65 (d, *J* = 6.9 Hz, 2H, Bz-py<sup>+</sup>), 8.02 (d, *J* = 6.4 Hz, 2H, py), 7.65–7.41 (m, 5H, benzyl), and 5.90 (s, 2H, CH<sub>2</sub>). The <sup>1</sup>H-NMR spectrum is provided in Figure S1.

A glass vial was charged with 1-benzyl-4,4'-bipyridinium bromide (3.00 g, 6.11 mmol), acetonitrile (5 mL), chloroform (15 mL), and acrylic acid (15 mL), and stirred for 24 h at 20 °C. The precipitate was filtered, washed by chloroform 3 times, and dried in vacuum. The obtained solid was dissolved in minimum amount of water, and a concentrated aqueous solution of NH<sub>4</sub>PF<sub>6</sub> (5 g; 30.5 mmol) was added to the solution. The white precipitate was filtered, washed by chloroform 3 times, and dried in vacuum to give Bz-V-Et(COOH) (975 mg; 1.60 mmol; 26% yield). <sup>1</sup>H-NMR (DMSO-*d*<sub>6</sub>; 400 MHz):  $\delta$  = 9.51 (d, *J* = 6.4 Hz, 2H, Bz-py<sup>+</sup>), 9.39 (d, *J* = 6.9 Hz, 2H, Et-py<sup>+</sup>), 8.77 (d, *J* = 6.4 Hz, 2H, Bz-py<sup>+</sup>), 8.74 (d, *J* = 6.4 Hz, 2H, Et-py<sup>+</sup>), 7.67–7.43 (m, 5H, benzyl), 5.94 (s, 2H, CH<sub>2</sub>), 4.89 (dd, *J* = 6.9, 6.4 Hz, 2H, CH<sub>2</sub>CH<sub>2</sub>), and 3.17 (dd, *J* = 6.9, 6.4 Hz, 2H, CH<sub>2</sub>CH<sub>2</sub>). The <sup>1</sup>H-NMR spectrum is provided in Figure S2.

### Synthesis of poly(NIPAAm-co-NAPMAm)

Poly(NIPAAm-co-NAPMAm) was synthesized by atom transfer radical polymerization (Scheme 1(b)). A glass vial was charged with NIPAAm (6.59 g; 58.2 mmol), NAPMAm (322 mg; 1.80 mmol) ([NIPAAm]:[NAPMAm] = 97:3), dimethylformamide (DMF) (10 mL), and water (10 mL) and purged with Ar for 30 min. Then, tris[2-(dimethylamino)ethyl]amine (Me<sub>6</sub>TREN) (53.4  $\mu$ L; 0.200 mmol) and CuBr (27.8 mg; 0.200 mmol) were added to the solution and purged with Ar for 3 min. Subsequently, ethyl 2-bromoisobutyrate (EBiB) (29.8  $\mu$ L; 0.200 mmol) was introduced, and the mixture was further purged with Ar for 3 min. Atom transfer radical polymerization was performed at 50 °C for 5 h. The monomer conversion rates of NIPAAm and NAPMAm were determined as ca. 46.5% and 67.9%, respectively, by analyzing an aliquot of the crude mixture with <sup>1</sup>H-NMR. The resulting solution was dialyzed against water and then lyophilized. The <sup>1</sup>H-NMR spectrum of the obtained polymer is provided in Figure S3.

### Synthesis of P(NIPAAm-co-NAPMAm-co-NAPMAmV) (poly(NIPAAm-V))

Poly(NIPAAm-V) was synthesized by post-polymerization modification of Poly(NIPAAm-co-

NAPMAm) (Scheme 1(b)). Poly(NIPAAm-co-NAPMAm) (500 mg; 30  $\mu$ mol), Bz-V-EtCOOH (169 mg; 277  $\mu$ mol), and dehydrated DMF (10 mL) were placed in a glass vial, and the solution was cooled in an ice bath. Subsequently, a mixture of 4-dimethylaminopyridine (DMAP) (37.5 mg; 307  $\mu$ mol) and 1-(3-dimethylaminopropyl)-3-ethylcarbodiimide hydrochloride (EDC) (212 mg; 1.11 mmol) in dehydrated DMF (10 mL) was added dropwise. The reaction mixture was warmed to 22 °C and stirred for 23 h. Afterward, the solution was dialyzed against methanol, and the solvent was evaporated. The residue was dissolved in a minimal amount of acetone and reprecipitated from hexane. The obtained solid was dried in vacuo to yield poly(NIPAAm-V). The introduction number of viologen moiety into the polymer chain was determined from the <sup>1</sup>H-NMR result. The <sup>1</sup>H-NMR spectrum of the obtained polymer is provided in Figure S4.

### Preparation of poly(NIPAAm-V) supporting platinum catalyst

A platinum catalyst for hydrogen evolution was synthesized according to the literature [40] with modifications. P(NIPAAm-V) (50 mg, 2.9  $\mu$ mol), K<sub>2</sub>PtCl<sub>4</sub> (8.28 mg; 20  $\mu$ mol), ethanol (8 mL), and water (2 mL) were placed in a round-bottom flask equipped with a reflux condenser. The reaction mixture was refluxed for 3 h. The solvent was evaporated, and the resulting solid was dispersed in acetate buffer solution (0.1 M; pH 5), yielding a dispersion of the polymer-supported platinum catalyst ([Pt] = 4.29 mg mL<sup>-1</sup>). The dispersion was stored in a refrigerator at 4 °C.

### Determination of lower critical solution temperatures of poly(NIPAAm-V) in oxidized and reduced states

A 0.1 wt% solution of poly(NIPAAm-V) in 0.1 M acetate buffer (pH 5) was prepared, and the transmittance at 900 nm was measured while increasing the temperature from 35 °C to 45 °C. The LCST of the oxidized form of poly(NIPAAm-V) was determined from the onset of the decrease in transmittance. A similar experiment was conducted for the reduced form: the above polymer solution was purged with Ar for 10 min, and then an aliquot of Na<sub>2</sub>S<sub>2</sub>O<sub>4</sub> (0.267 mg, 1.53  $\mu$ mol, 11 equiv. relative to the viologen moiety) was added to reduce the viologen units. The temperature was again ramped from 35 °C to 45 °C, and the transmittance at 900 nm was recorded to determine the LCST in the reduced state.

### Chemically-fueled phase transition

A 0.1 wt% solution of poly(NIPAAm-V) (58  $\mu$ M) in 0.1 M acetate buffer (pH 5) was combined with the platinum catalyst described above in a cuvette sealed with a septum



cap. The solution was purged with Ar for 10 min and then allowed to equilibrate at the measurement temperature in the DLS instrument for an additional 10 min. The hydrodynamic diameter at time zero was determined by DLS. Separately, 4.00 mL of 0.1 M acetate buffer (pH 5) was purged with Ar for 10 min, and 30.1 mg (172  $\mu\text{mol}$ ) of  $\text{Na}_2\text{S}_2\text{O}_4$  was added to prepare a 43.3 mM stock solution of the reducing agent. From this stock solution, 10  $\mu\text{L}$  (0.43  $\mu\text{mol}$ , 3 equiv. relative to the viologen moiety) was injected via a gas-tight syringe into the poly(NIPAAm-V) solution, and the time course of the hydrodynamic diameter was recorded by DLS. The data were converted into hydrodynamic diameter histograms using Contin analysis, and the diameter of the dominant scattering species was plotted as a function of time. In some experiments, the residual amount of viologen radicals in the post-reaction solution was estimated by referring to the absorbance at 554 nm at 20  $^{\circ}\text{C}$ . Additionally, hydrogen gas evolved in the headspace of the cuvette after the reaction was quantified by GC analysis. The size at the steady state was calculated by averaging the hydrodynamic diameter in the flat region of the time-course graph. The lifetime was defined as the time at which the hydrodynamic diameter became less than half of its steady-state value. The movie of the chemically-fueled phase transition was recorded using a CS500-C camera equipped with a SHODENSHA SDS-M19 lens, while the temperature of the reaction solution in a cuvette was controlled using a UNISOKU CoolSpeK USP-203 system. To visualize aggregate formation, green laser light (532 nm) was irradiated from the left side of the cuvette during the measurement. The video is presented at 90  $\times$  speed.

## Results and discussion

### Synthesis of poly(NIPAAm)-based polymer bearing viologen moieties

We synthesized the target viologen-containing polymer, P (NIPAAm-V), by coupling a viologen

derivative (BzVetCOOH) with PNIPAAm bearing amino groups (Scheme 1). BzVetCOOH was prepared via stepwise alkylation of 4,4'-bipyridine, following reported procedures [38,39]. PNIPAAm containing amino groups was obtained by the copolymerization of NIPAAm and NAPMAm, yielding poly(NIPAAm<sub>113</sub>-co-NAPMAm<sub>6,1</sub>), as confirmed by  $^1\text{H-NMR}$  spectroscopy. Subsequently, condensation of BzVetCOOH with poly(NIPAAm<sub>113</sub>-co-NAPMAm<sub>6,1</sub>) using EDC afforded the viologen-functionalized polymer, poly(NIPAAm-V). The appearance of peaks assignable to the viologen structure in the  $^1\text{H-NMR}$  spectra (8.0–9.6 ppm) demonstrated the successful introduction of viologen. From the integral values, we estimated that each polymer chain contained  $\sim 1.2$  viologen units, leading to the final composition poly(NIPAAm<sub>113</sub>-co-NAPMAm<sub>4,9</sub>-co-NAPMAmV<sub>1,2</sub>).

### Phase transition of poly(NIPAAm-V) in oxidized and reduced states

Figure 2(a) illustrates the absorption spectra of poly(NIPAAm-V) under oxidized and reduced conditions at 20  $^{\circ}\text{C}$  in acetate buffer (0.1 M, pH 5). Under the reduced condition, the spectrum exhibited specific sharp peaks at 368 and 399 nm and broad peaks around 554 and 886 nm. Notably, the spectrum of the reduced polymer closely resembled that of the viologen radical  $\pi$ -dimer [41] rather than the monomeric form, suggesting that the viologen moieties primarily exist in a dimerized radical form. This result suggests that both the hydrophobic interactions of the PNIPAAm main chain and the  $\pi$ - $\pi$  interactions among viologen units contribute to polymer aggregation under reducing conditions.

Figure 2(b) shows the temperature-dependent transmittance of poly(NIPAAm-V) solutions under both oxidized and reduced conditions. Here, it should be noted that the transmittance in the reduced state was

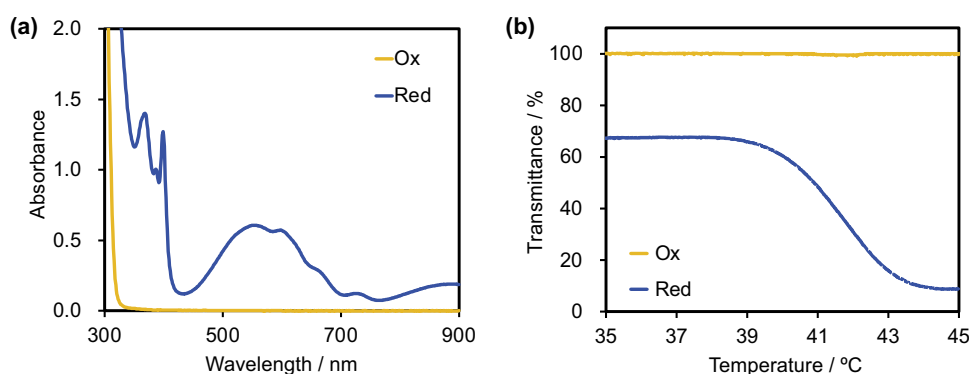


**Figure 2.** (a) UV-Vis absorption spectra of poly(NIPAAm-V) ([poly(NIPAAm-V)] = 1.0 g/L) in 0.1 M acetate buffer (pH 5) at 20  $^{\circ}\text{C}$  in the presence and absence of a reductant ( $[\text{Na}_2\text{S}_2\text{O}_4] = 0.77$  mM, 11 equiv. relative to the viologen moiety). (b) Temperature dependence of optical transmittance at 900 nm in a 0.1 M acetate buffer solution (pH 5) containing poly(NIPAAm-V) ([poly(NIPAAm-V)] = 1.0 g/L) at 20  $^{\circ}\text{C}$  in the presence and absence of a reductant ( $[\text{Na}_2\text{S}_2\text{O}_4] = 0.77$  mM, 11 equiv. relative to the viologen moiety). Transmittances were measured at 900 nm.

approximately 70% at 30 °C, which is below its LCST, due to spectral overlap between the absorption band of the reduced viologen moieties and the measurement wavelength (900 nm). Under oxidizing conditions, only a slight decrease ( $\sim 1\%$ ) in transmittance was observed around 41 °C (Figure S5). Comparison with the poly(NIPAAm-*co*-NAPMAm) copolymer revealed a similar transition temperature (Figure S5), suggesting that some fraction of the polymer chains did not carry a viologen unit. This arises from the average viologen incorporation of only  $\sim 1.2$  per chain; hence, chains lacking viologen moieties can exhibit typical PNIPAAm-like transitions near 41 °C. Attempts to increase viologen content beyond 1.2 units per chain were unsuccessful; hence, the present sample contained traces of P(NIPAAm-*co*-NAPMAm). Apart from this minor transition, no distinct LCST-like behavior was observed up to 45 °C, implying that fully viologen-bearing chains exhibit LCSTs above 45 °C in the oxidized state.

In contrast, under reducing conditions, a distinct decrease in transmittance was observed at 40 °C. Thus, the LCST for the reduced form of poly(NIPAAm-V) was determined to be 40 °C. Reduction of viologen from the 2+ to 1+ state presumably increases hydrophobicity, causing a negative shift of the LCST. Because the LCSTs of the oxidized and reduced polymer differ by several degrees, the polymer remains soluble random coil state or aggregated globule state within a bistable temperature range depending on viologen's redox state. This redox-responsive LCST shift is crucial for coupling the polymer's conformational changes with an external redox reaction cycle.

### Chemically-fueled phase transition of poly(NIPAAm-V)

Based on LCST measurements, we selected 42 °C, for the chemically-fueled phase transition experiments, as it falls within the presumed bistable range. Video S1 shows the time course of poly(NIPAAm-V) (0.1 wt%;

58  $\mu\text{M}$ ) dispersed in acetate buffer (0.1 M, pH 5) containing the platinum catalyst ( $[\text{Pt}] = 3.3 \text{ ppm}$ ) at 42 °C. In this experiment, a green laser was illuminated from left to right to visualize aggregate formation via light scattering. After the addition of the reductant, the solution turned deep purple and gradually returned to a colorless state over time. This sequential change is a signature of chemically-fueled processes. While the laser beam path was not visible prior to reduction, the formation of aggregates became evident from the appearance of a light-scattering path following reductant addition. However, due to the intense coloration of the solution, the beam path became indistinguishable a few minutes after reduction. Figure 3(a) shows the time evolution of the hydrodynamic diameter of the poly(NIPAAm-V) dispersion measured by DLS. A small population of 90 nm aggregates existed before reducing-agent addition, likely derived from trace P(NIPAAm-*co*-NAPMAm) chains having a lower LCST (41 °C). Immediately after the addition of the reducing agent  $\text{Na}_2\text{S}_2\text{O}_4$  at 0.22 mM, rapid formation of large polymer assemblies was observed. These assemblies continued to grow until reaching a steady-state size of approximately 582 nm. After a certain lifetime, these assemblies abruptly collapsed, reverting to the initial solution state. In the absence of the platinum catalyst, the aggregation proceeded continuously up to 1400 nm, and the particles did not revert to smaller sizes. These results suggest that the Pt catalyst drives the oxidation and disassembly of the polymer as well as the consumption of the reductant. Gas chromatographic analysis of the headspace gas in the reaction cuvette, 60 min after adding the reducing agent showed that hydrogen gas was evolved only in the presence of the Pt catalyst (Figure 3(b)). Furthermore, UV – Vis absorption measurements revealed that only 4.1% of the viologen radicals remained after 60 min with the Pt catalyst, whereas 77.0% of the radicals persisted in the absence of Pt (Figure 3(c)). These observations confirm that the Pt-catalyzed hydrogen evolution reaction consumes the

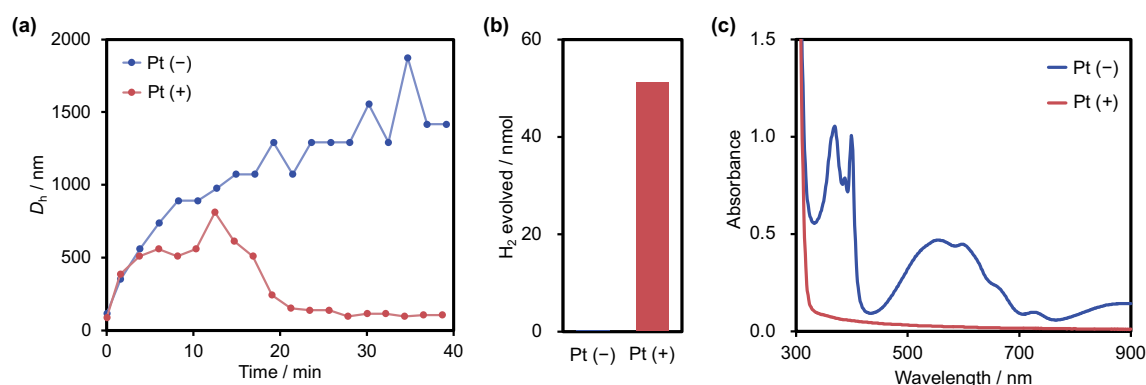


**Figure 3.** (a) Time profiles of hydrodynamic diameters, (b) Evolved hydrogen gas, and (c) UV-Vis absorption spectra of poly(NIPAAm-V) solutions with and without Pt catalyst after the addition of a reductant at 20 °C. Conditions: [poly(NIPAAm-V)] = 1.0 g/L,  $[\text{Na}_2\text{S}_2\text{O}_4] = 0.22 \text{ mM}$  (3 equiv. relative to the viologen moiety),  $[\text{Pt}] = 3.3 \text{ ppm}$ , 0.1 M acetate buffer (pH 5), 42 °C.

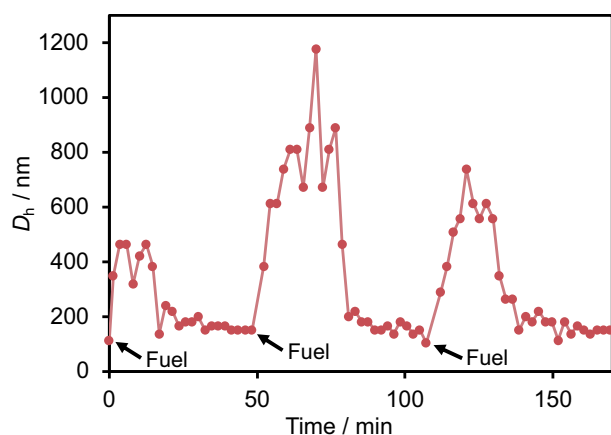


**Figure 4.** Time profile of hydrodynamic diameters in poly (NIPAAm-V) solutions following three consecutive additions of  $\text{Na}_2\text{S}_2\text{O}_4$ . Fuel:  $[\text{Na}_2\text{S}_2\text{O}_4] = 0.22 \text{ mm}$  (3 equiv. relative to the viologen moiety). Conditions:  $[\text{poly}(\text{NIPAAm-V})] = 1.0 \text{ g/L}$ ,  $0.1 \text{ M}$  acetate buffer (pH 5),  $[\text{pt}] = 3.3 \text{ ppm}$ .

reducing power in the solution, thereby oxidizing the viologen radicals and reverting the polymer to its more hydrophilic oxidized state. Accordingly, we conclude that chemically-fueled phase transition occurs in this system by coupling the chemical reduction of viologen moieties with the platinum-catalyzed hydrogen evolution reaction. The dissipation of chemical energy as hydrogen evolution manifests as transient polymer aggregation, ultimately returning the system to the oxidized, dispersed state. Additionally, repeated additions of the reductant were performed to investigate the cyclability of the chemically-fueled phase transition (Figure 4). Although the aggregates formed during the second and third cycles were slightly larger than those observed in the first cycle, the system consistently exhibited spontaneous aggregation – dispersion behavior (Figure 4). These results demonstrate that the system can undergo multiple cycles of the chemically-fueled phase transitions.

### Control of the chemically-fueled phase transition by catalyst concentration

A key advantage of this catalyst-driven energy dissipation scheme lies in its tunability. By varying the amount of platinum catalyst, we can modulate the kinetics of viologen oxidation and hydrogen evolution. Figure 5(a) summarizes the time evolution of the aggregate size at different platinum concentrations (0–6.6 ppm). As the Pt concentration increases, the steady-state aggregate size clearly decreases (Figure 5(b)), indicating that faster oxidation of the viologen radicals leads to smaller aggregates. These results are consistent with accelerated oxidation of reduced viologen, which promotes faster polymer chain hydration and dissociation. Furthermore, the lifetimes of the polymer assemblies shorten at higher Pt concentration, reflecting the accelerated consumption of the

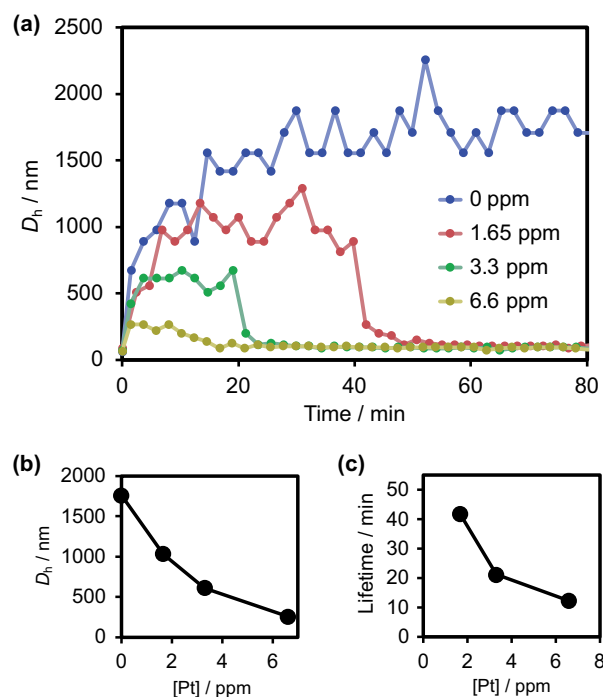


**Figure 5.** (a) Time profiles of hydrodynamic diameters in poly (NIPAAm-V) solutions with varying Pt catalyst loadings after the addition of a reductant. Conditions:  $[\text{poly}(\text{NIPAAm-V})] = 1.0 \text{ g/L}$ ,  $[\text{Na}_2\text{S}_2\text{O}_4] = 0.22 \text{ mm}$  (3 equiv. relative to the viologen moiety),  $0.1 \text{ M}$  acetate buffer (pH 5),  $42^\circ\text{C}$ . (b) Dependence of hydrodynamic diameters on Pt catalyst loadings. (c) Dependence of lifetimes of chemically-fueled phase transition on Pt catalyst loadings.

reducing agent by the Pt catalyst (Figure 5(c)). These data clearly demonstrate that the size and lifetime of the aggregates are regulated by the kinetics of the reaction cycle and can be easily controlled by adjusting the platinum catalyst concentration.

### Control of the chemically-fueled phase transition by temperature

In addition to catalyst concentration, temperature also influences the reaction kinetics and the polymer's aggregation behavior. Generally, higher temperatures accelerate catalytic reactions but also promote dehydration of PNIPAAm-based polymers above their LCST [28]. To clarify the combined impact of these factors, we monitored the chemically-fueled phase transition at various temperatures ranging from  $40^\circ\text{C}$  to  $46^\circ\text{C}$  (Figure 6(a)). We found that the steady-state aggregate size increased with temperature (Figure 6(b)), suggesting that the enhanced hydrophobicity of PNIPAAm segments at higher temperatures primarily governed the growth of the polymer aggregate. In contrast, the lifetime of the aggregates decreases with increasing temperature (Figure 6(c)), likely due to accelerated hydrogen evolution and consequently faster depletion of the reducing agent. The result implies the lifetime is

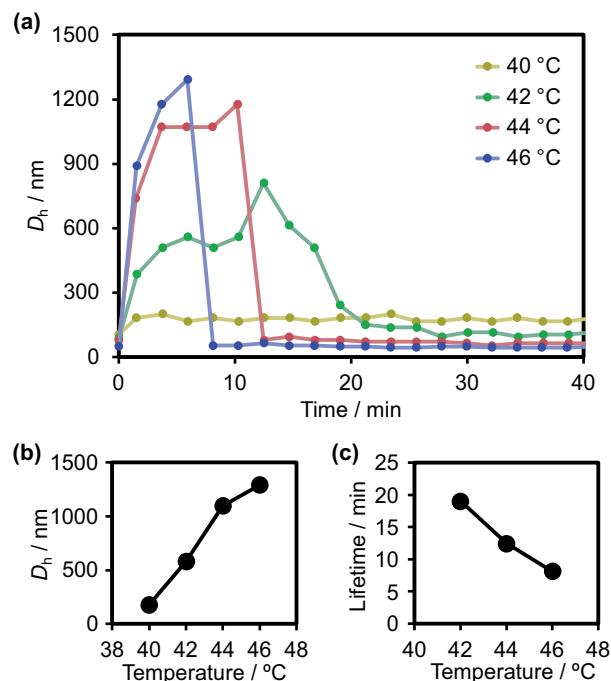


**Figure 6.** (a) Time profiles of hydrodynamic diameters in poly(NIPAAm-V) solutions at varying reaction temperatures after the addition of a reductant. Conditions: [poly(NIPAAm-V)] = 1.0 g/L, [Na<sub>2</sub>S<sub>2</sub>O<sub>4</sub>] = 0.22 mm (3 equiv. relative to the viologen moiety), 0.1 M acetate buffer (pH 5), [pt] = 3.3 ppm. (b) Dependence of hydrodynamic diameters on temperature. (c) Dependence of lifetimes of chemically-fueled phase transition on temperature.

mainly dominated by reaction kinetics. These findings highlight the competing roles of temperature in governing both polymer dehydration and catalytic reaction rates, resulting in temperature-dependent spatiotemporal evolution of the assemblies.

## Conclusions

We have developed a chemically-fueled phase transition system based on redox-responsive PNIPAAm bearing viologen moieties, coupled with a Pt catalyst for hydrogen evolution. In this system, viologen units are reduced by a chemical fuel, Na<sub>2</sub>S<sub>2</sub>O<sub>4</sub>, triggering coil-to-globule transitions in the polymer. These reduced viologen radicals subsequently donate electrons to the platinum catalyst, driving hydrogen gas evolution and oxidation of the polymer back to its random coil state. This cyclic redox process enables transient formation of polymer assemblies with tunable sizes and lifetimes, reminiscent of biological systems that harness high-energy molecules to induce and regulate macromolecular assemblies. Moreover, by modulating the platinum catalyst concentration and the reaction temperature, we demonstrated precise control over both the size and lifetime of the aggregates. Our findings highlight the feasibility of constructing dynamic polymer systems that replicate, in part, nature's strategy of orchestrating

macromolecular assemblies via energy-dissipative chemical reaction networks. We anticipate that chemically-fueled phase transition approaches will find broad applications in designing next-generation soft materials capable of reversible and spatiotemporal morphological changes, thereby advancing the frontier of biomimetic and autonomous materials science.

## Disclosure statement

No potential conflict of interest was reported by the author(s).

## Funding

This work was partially supported by a Grant-in-Aid for Young Scientists Grant Number [JP23K13797] to T. E., and a Grant-in-Aid for Scientific Research Grant Number [JP20H00388] to R. Y. from the Ministry of Education, Culture, Sports, Science, and Technology of Japan. Japan Society for the Promotion of Science [JP23K13797, JP20H00388].

## ORCID

Ryo Yoshida  <http://orcid.org/0000-0002-0558-2922>

## References

- [1] Brouhard GJ, Rice LM. Microtubule dynamics: an interplay of biochemistry and mechanics. *Nat Rev Mol Cell Biol.* 2018;19(7):451–463. doi: 10.1038/s41580-018-0009-y
- [2] Akhmanova A, Steinmetz MO. Control of microtubule organization and dynamics: two ends in the limelight. *Nat Rev Mol Cell Biol.* 2015;16(12):711–726. doi: 10.1038/nrm4084
- [3] Kühner S, Fischer S. Structural mechanism of the ATP-induced dissociation of rigor myosin from actin. *Proc Natl Acad Sci USA.* 2011;108(19):7793–7798. doi: 10.1073/pnas.1018420108
- [4] Korn ED. Actin polymerization and its regulation by proteins from nonmuscle cells. *Physiol Rev.* 1982;62(2):672–737. doi: 10.1152/physrev.1982.62.2.672
- [5] Disanza A, Steffen A, Hertzog M, et al. Actin polymerization machinery: the finish line of signaling networks, the starting point of cellular movement. *Cell Mol Life Sci.* 2005;62(9):955–970. doi: 10.1007/s00018-004-4472-6
- [6] Dominguez R, Holmes KC. Actin structure and function. *Annu Rev Biophys.* 2011;40(1):169–186. doi: 10.1146/annurev-biophys-042910-155359
- [7] Das K, Gabrielli L, Prins LJ. Chemically fueled self-assembly in biology and chemistry. *Angew Chem Int Ed.* 2021;60(37):20120–20143. doi: 10.1002/anie.202100274
- [8] Trivedi DV, Nag S, Spudich A, et al. The myosin family of mechanoenzymes: from mechanisms to therapeutic approaches. *Annu Rev Biochem.* 2020;89(1):667–693. doi: 10.1146/annurev-biochem-011520-105234
- [9] Karplus M, Kuriyan J. Molecular dynamics and protein function. *Proc Natl Acad Sci USA.* 2005;102(19):6679–6685. doi: 10.1073/pnas.0408930102



- [10] Ashkenasy G, Hermans TM, Otto S, et al. Systems chemistry. *Chem Soc Rev*. 2017;46(9):2543–2554. doi: [10.1039/c7cs00117g](https://doi.org/10.1039/c7cs00117g)
- [11] Sharko A, Livitz D, De Piccoli S, et al. Insights into chemically fueled supramolecular polymers. *Chem Rev*. 2022;122(13):11759–11777. doi: [10.1021/acs.chemrev.1c00958](https://doi.org/10.1021/acs.chemrev.1c00958)
- [12] Chen X, Würbser MA, Boekhoven J. Chemically fueled supramolecular materials. *Acc Mater Res*. 2023;4(5):416–426. doi: [10.1021/accountsmr.2c00244](https://doi.org/10.1021/accountsmr.2c00244)
- [13] Kriebisch BAK, Jussupow A, Bergmann AM, et al. Reciprocal coupling in chemically fueled assembly: a reaction cycle regulates self-assembly and vice versa. *J Am Chem Soc*. 2020;142(49):20837–20844. doi: [10.1021/jacs.0c10486](https://doi.org/10.1021/jacs.0c10486)
- [14] Dai K, Fores JR, Wanzke C, et al. Regulating chemically fueled peptide assemblies by molecular design. *J Am Chem Soc*. 2020;142(33):14142–14149. doi: [10.1021/jacs.0c04203](https://doi.org/10.1021/jacs.0c04203)
- [15] Schnitter F, Bergmann AM, Winkeljann B, et al. Synthesis and characterization of chemically fueled supramolecular materials driven by carbodiimide-based fuels. *Nat Protoc*. 2021;16(8):3901–3932. doi: [10.1038/s41596-021-00563-9](https://doi.org/10.1038/s41596-021-00563-9)
- [16] Wanzke C, Tena-Solsona M, Rieß B, et al. Active droplets in a hydrogel release drugs with a constant and tunable rate. *Mater Horiz*. 2020;7(5):1397–1403. doi: [10.1039/C9MH01822K](https://doi.org/10.1039/C9MH01822K)
- [17] Zambrano P, Chen X, Kriebisch CME, et al. Chemically driven division of protocells by membrane budding. *J Am Chem Soc*. 2024;146(49):33359–33367. doi: [10.1021/jacs.4c08226](https://doi.org/10.1021/jacs.4c08226)
- [18] Leira-Iglesias J, Tassoni A, Adachi T, et al. Oscillations, travelling fronts and patterns in a supramolecular system. *Nat Nanotechnol*. 2018;13(11):1021–1027. doi: [10.1038/s41565-018-0270-4](https://doi.org/10.1038/s41565-018-0270-4)
- [19] Selmani S, Schwartz E, Mulvey JT, et al. Electrically fueled active supramolecular materials. *J Am Chem Soc*. 2022;144(17):7844–7851. doi: [10.1021/jacs.2c01884](https://doi.org/10.1021/jacs.2c01884)
- [20] Barpuzary D, Hurst PJ, Patterson JP, et al. Waste-free fully electrically fueled dissipative self-assembly system. *J Am Chem Soc*. 2023;145(6):3727–3735. doi: [10.1021/jacs.2c13140](https://doi.org/10.1021/jacs.2c13140)
- [21] Chen XM, Hou XF, Bisoyi HK, et al. Light-fueled transient supramolecular assemblies in water as fluorescence modulators. *Nat Commun*. 2021;12(1):1–8. doi: [10.1038/s41467-021-25299-8](https://doi.org/10.1038/s41467-021-25299-8)
- [22] Hou XF, Chen XM, Bisoyi HK, et al. Light-driven aqueous dissipative pseudorotaxanes with tunable fluorescence enabling deformable nano-assemblies. *ACS Appl Mater Interfaces*. 2023;15(8):11004–11015. doi: [10.1021/acsami.2c20276](https://doi.org/10.1021/acsami.2c20276)
- [23] Maiti S, Fortunati I, Ferrante C, et al. Dissipative self-assembly of vesicular nanoreactors. *Nat Chem*. 2016;8(7):725–731. doi: [10.1038/nchem.2511](https://doi.org/10.1038/nchem.2511)
- [24] Cardona MA, Prins LJ. ATP-fuelled self-assembly to regulate chemical reactivity in the time domain. *Chem Sci*. 2020;11(6):1518–1522. doi: [10.1039/C9SC05188K](https://doi.org/10.1039/C9SC05188K)
- [25] Wu C, Wang X. Globule-to-coil transition of a single homopolymer chain in solution. *Phys Rev Lett*. 1998;80(18):4092–4094. doi: [10.1103/PhysRevLett.80.4092](https://doi.org/10.1103/PhysRevLett.80.4092)
- [26] Baysal BM, Karasz FE. Coil-globule collapse in flexible macromolecules. *Macromol Theory Simul*. 2003;12(9):627–646. doi: [10.1002/mats.200350028](https://doi.org/10.1002/mats.200350028)
- [27] Podewitz M, Wang Y, Quoika PK, et al. Coil-globule transition thermodynamics of poly(N-isopropylacrylamide). *J Phys Chem B*. 2019;123(41):8838–8847. doi: [10.1021/acs.jpcc.9b06125](https://doi.org/10.1021/acs.jpcc.9b06125)
- [28] Halperin A, Kröger M, Winnik FM. Poly(N-isopropylacrylamide)-phase diagrams: 50 years of research. *Angew Chem*. 2015;127(51):15558–15586. doi: [10.1002/ange.201506663](https://doi.org/10.1002/ange.201506663)
- [29] Das A, Babu A, Chakraborty S, et al. Poly(N-isopropylacrylamide) and its copolymers: a review on recent advances in the areas of sensing and biosensing. *Adv Funct Mater*. 2024;(37). doi: [10.1002/adfm.202402432](https://doi.org/10.1002/adfm.202402432)
- [30] Lanzalaco S, Armelin E. Poly(N-isopropylacrylamide) and copolymers: a review on recent progresses in biomedical applications. *Gels*. 2017;3(4):36. doi: [10.3390/gels3040036](https://doi.org/10.3390/gels3040036)
- [31] Li L, Scheiger JM, Levkin PA. Design and applications of photoresponsive hydrogels. *Adv Mater*. 2019;31(26). doi: [10.1002/adma.201807333](https://doi.org/10.1002/adma.201807333)
- [32] Chen R, Wang H, Doucet M, et al. Thermo-electro-responsive redox-copolymers for amplified solvation, morphological control, and tunable ion interactions. *JACS Au*. 2023;3(12):3333–3344. doi: [10.1021/jacsau.3c00486](https://doi.org/10.1021/jacsau.3c00486)
- [33] Homma K, Chang AC, Yamamoto S, et al. Design of azobenzene-bearing hydrogel with photoswitchable mechanics driven by photo-induced phase transition for in vitro disease modeling. *Acta Biomater*. 2021;132:103–113. doi: [10.1016/j.actbio.2021.03.028](https://doi.org/10.1016/j.actbio.2021.03.028)
- [34] Okeyoshi K, Yoshida R. Polymeric design for electron transfer in photoinduced hydrogen generation through a coil-globule transition. *Angew Chem Int Ed*. 2019;58(22):7304–7307. doi: [10.1002/anie.201901666](https://doi.org/10.1002/anie.201901666)
- [35] Hagiwara R, Yoshida R, Okeyoshi K. Bioinspired hydrogels: polymeric designs towards artificial photosynthesis. *Chem Commun*. 2024;60(91):13314–13324. doi: [10.1039/D4CC04033C](https://doi.org/10.1039/D4CC04033C)
- [36] Harriman A, Porter G. Viologen/Platinum systems for hydrogen generation. *J Chem Soc Faraday Trans 2*. 1982;78(11):1937. doi: [10.1039/f29827801937](https://doi.org/10.1039/f29827801937)
- [37] Matheson MS, Lee PC, Meisel D, et al. Kinetics of hydrogen production from methyl viologen radicals on colloidal platinum. *J Phys Chem*. 1983;87(3):394–399. doi: [10.1021/j100226a008](https://doi.org/10.1021/j100226a008)
- [38] Suzuki W, Kotani H, Ishizuka T, et al. A diprotonated porphyrin as an electron mediator in photoinduced electron transfer in hydrogen-bonded supramolecular assemblies. *J Phys Chem C*. 2019;123(18):11529–11538. doi: [10.1021/acs.jpcc.9b02449](https://doi.org/10.1021/acs.jpcc.9b02449)
- [39] Zhang X, Xu Y, Yang Y, et al. A new signal-on photoelectrochemical biosensor based on a graphene/quantum-dot nanocomposite amplified by the dual-quenched effect of bipyridinium relay and AuNPs. *Chem Eur J*. 2012;18(51):16411–16418. doi: [10.1002/chem.201202213](https://doi.org/10.1002/chem.201202213)
- [40] Yu W, Lou LL, Li S, et al. Highly efficient and durable platinum nanocatalysts stabilized by thiol-terminated poly(N-isopropyl acrylamide) for selective hydrogenation of halonitrobenzene to haloaniline. *RSC Adv*. 2017;7(2):751–757. doi: [10.1039/C6RA24773C](https://doi.org/10.1039/C6RA24773C)
- [41] Geraskina MR, Dutton AS, Juetten MJ, et al. The viologen cation radical pimer: a case of dispersion-driven bonding. *Angew Chem Int Ed*. 2017;56(32):9435–9439. doi: [10.1002/anie.201704959](https://doi.org/10.1002/anie.201704959)